Chemical Science

ROYAL SOCIETY OF CHEMISTRY

EDGE ARTICLE

View Article Online
View Journal | View Issue

Cite this: *Chem. Sci.*, 2023, **14**, 7327

All publication charges for this article have been paid for by the Royal Society of Chemistry

Targeted proximity-labelling of protein tyrosines *via* flavin-dependent photoredox catalysis with mechanistic evidence for a radical–radical recombination pathway†

Taylor O. Hope,[a] Tamara Reyes-Robles,[b] Keun Ah Ryu,[b] Steven Mauries,[a] Nicole Removski,[a] Jacinthe Maisonneuve,[a] Rob C. Oslund, ‡*[b] Olugbeminiyi O. Fadeyi‡*[b] and Mathieu Frenette *[a]

Received 3rd February 2023
Accepted 17th May 2023

DOI: 10.1039/d3sc00638g

rsc.li/chemical-science

Flavin-based photocatalysts such as riboflavin tetraacetate (**RFT**) serve as a robust platform for light-mediated protein labelling *via* phenoxy radical-mediated tyrosine–biotin phenol coupling on live cells. To gain insight into this coupling reaction, we conducted detailed mechanistic analysis for **RFT**-photomediated activation of phenols for tyrosine labelling. Contrary to previously proposed mechanisms, we find that the initial covalent binding step between the tag and tyrosine is not radical addition, but rather radical–radical recombination. The proposed mechanism may also explain the mecha-nism of other reported tyrosine-tagging approaches. Competitive kinetics experiments show that phenoxyl radicals are generated with several reactive intermediates in the proposed mechanism—primarily with the excited riboflavin-photocatalyst or singlet oxygen—and these multiple pathways for phenoxyl radical generation from phenols increase the likelihood of radical–radical recombination.

Introduction

Technologies that identify interacting proteins are crucial to understand fundamental biological processes and to enable new drug target discoveries. Visible light photocatalysis has emerged as an attractive platform for this purpose to achieve selective chemical transformations on and within biological materials with spatiotemporal control.[1–11] A key feature is that visible light selectively excites a photocatalyst; the excited photocatalyst then activates chemical tags for covalent protein labelling. Tag molecules are usually activated to become reactive intermediates with short lifetimes, such as radicals,[10,11] carbenes,[8] or nitrenes,[9] to limit the labelling radius within a complex biological environment. Importantly, a single photocatalyst can activate multiple tags resulting in substantial signal amplification for labelling with bioorthogonal handles such as biotin, azides, alkynes, or fluorophores for downstream protein analysis.[1,12]

A major trend in proximity protein tagging is to exploit the reactivity of tyrosine at a protein's surface. Notably, peroxidase-enabled tyrosine labelling has been developed for profiling protein environments in numerous cellular contexts.[13] In this system initiated by exogenous hydrogen peroxide, a phenol-containing tag is oxidized to phenoxyl radicals by heme-containing peroxidases resulting in the labelling of nearby proteins. Recently, we reported the use of a flavin-derived cofactor, riboflavin tetraacetate (**RFT**), as a photocatalyst for the generation of phenoxyl radical intermediates for tyrosine-based protein labelling (Fig. 1A).[4] Blue-light activated **RFT** was shown to achieve proximity labelling of proteins, live cells, and cell–cell contact regions (Fig. 1B). Similar to other reported tyrosine tagging methods, radical addition onto a neutral tyrosine is traditionally proposed as a key step in the mechanism.[10,11,14–16] However, to date, no direct evidence has been reported for this mechanism. Here, we examine the proposed radical addition mechanism and a competing radical–radical recombination pathway (Fig. 1C).

Results and discussion

Prior to exploring the mechanistic basis of **RFT**-mediated phenol–phenol coupling, we developed a novel proteomic workflow to evaluate the effect of targeted activation of **RFT** in a localized microenvironment. Having previously demonstrated by flow cytometry and confocal imaging that we can achieve

[a]*Department of Chemistry, NanoQAM, Centre Québécois des Matériaux Fonctionnels (CQMF), Université du Québec à Montréal, Montréal, Québec, H3C 3P8, Canada. E-mail: frenette.mathieu@uqam.ca*

[b]*Exploratory Science Center, Merck & Co., Inc., Cambridge, MA, USA. E-mail: niyi@induprolabs.com; rob@induprolabs.com*

† Electronic supplementary information (ESI) available. See DOI: https://doi.org/10.1039/d3sc00638g

‡ Current address: InduPro, Cambridge, Massachusetts, USA.

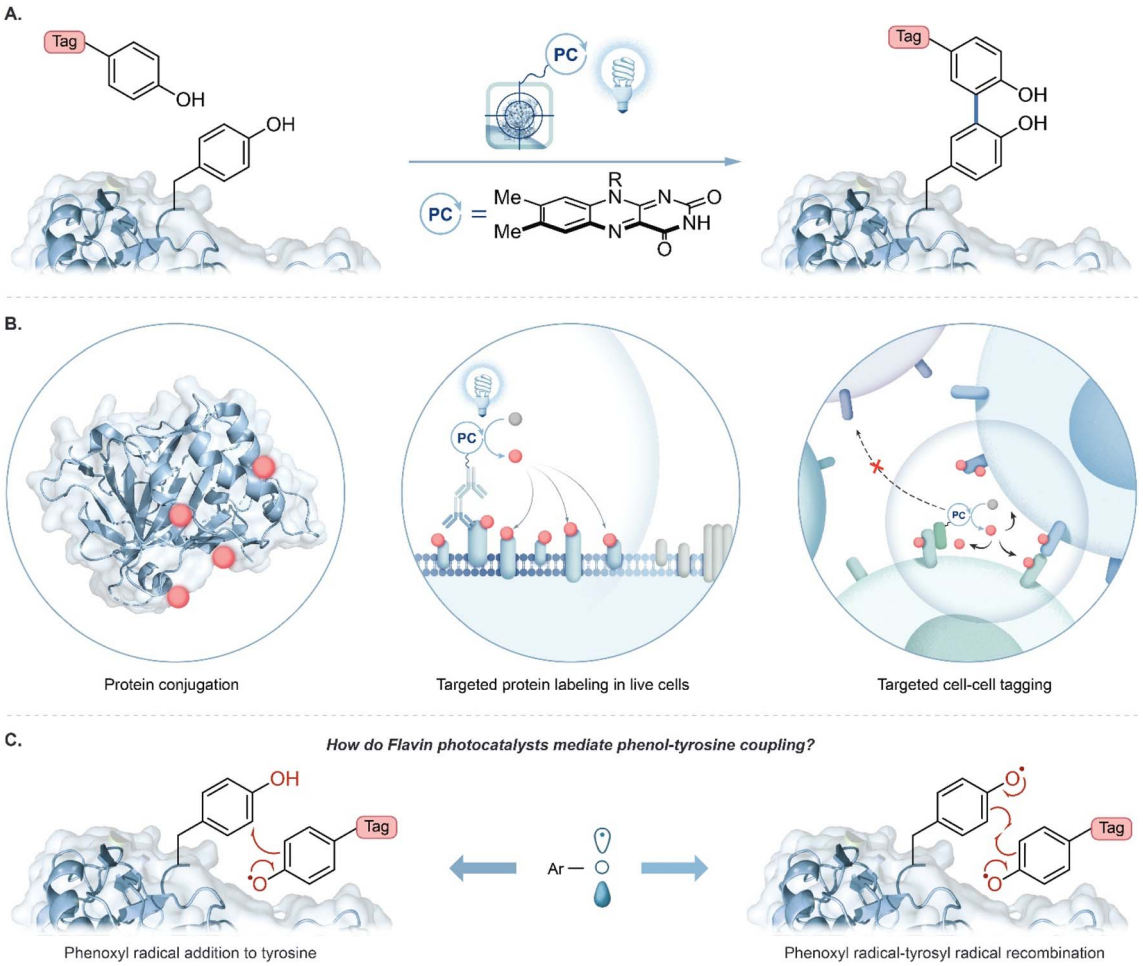

Fig. 1 (A) Flavin-based photocatalytic tyrosine-tagging by phenol containing tags. (B) Biological applications of RFT-mediated photocatalysis in protein and cellular environments. (C) Competing mechanistic proposals for the labelling of tyrosine by phenoxyl radicals: radical addition to tyrosine *versus* radical recombination.

RFT-mediated protein labelling on live cells,[4] this proteomic workflow focused on the evaluation of targeted *versus* untargeted activation of **RFT** localized to the cell surface (Fig. 2A). In these experiments, **RFT** was conjugated to a secondary antibody that can bind to a primary antibody recognizing cell surface proteins. We selected PTPRC (CD45), a T cell marker highly expressed on the cell surface,[17] as our target.

Accordingly, targeted delivery of **RFT** to PTPRC *via* the primary/secondary antibody system, followed by irradiation with blue light in the presence of biotin tyramide led to detection of PTPRC among the highest enriched proteins (Fig. 2B). Known PTPRC interactors such as the PTPRC associated protein (PTPRCAP), CD2, and LCK were also highly co-enriched with PTPRC (Fig. 2B and S1†). In contrast, untargeted delivery of free **RFT** catalysts to live cells (Fig. 2A) followed by irradiation with blue light in the presence of biotin tyramide failed to enrich PTPRC (Fig. 2B). Since the peroxidase enzyme similarly leverages biotin tyramide to achieve protein labelling,[13] we compared our **RFT** protein system to peroxidase-based labelling of CD45 on live cells followed by mass spectrometry based proteomic analysis. We observed a nearly three-fold increase in total protein enrichment using peroxidase-based labelling compared to **RFT** (Fig. 2C and S2†) suggesting a much larger effective labelling radius achieved by the enzyme-based method. Collectively these results highlight the ability of targeted activation of **RFT** to achieve localized phenoxyl radical tagging within complex cellular systems.

Likewise, tyrosine radical addition onto a neutral aromatic system has been proposed (Fig. 1C).[10,14] In both cases, prohibitively large activation energies are calculated for these proposed mechanisms (Tables S12 and S15†). A major contribution of this study is to bring convincing evidence against radical addition to tyrosine; the thermodynamic cost of this radical addition step is prohibitively unfavorable (Fig. 3A, $\Delta G_{DFT} > 34$ kcal mol^{-1}, Table S10†). The recombination of phenoxyl radicals, however, is much more probable (Fig. 3B, $\Delta G_{DFT} = -1$ to +3 kcal mol^{-1}, Table S9†). The slight endergonic recombination is a testament to phenoxyl radical stability—of course, the initial recombination product will rapidly tautomerize to regenerate aromaticity for a largely favorable end-product ($\Delta G_{DFT} = -36$ kcal mol^{-1}, Table S9†). Photocatalysis often employs metal-based complexes due to their long-lived

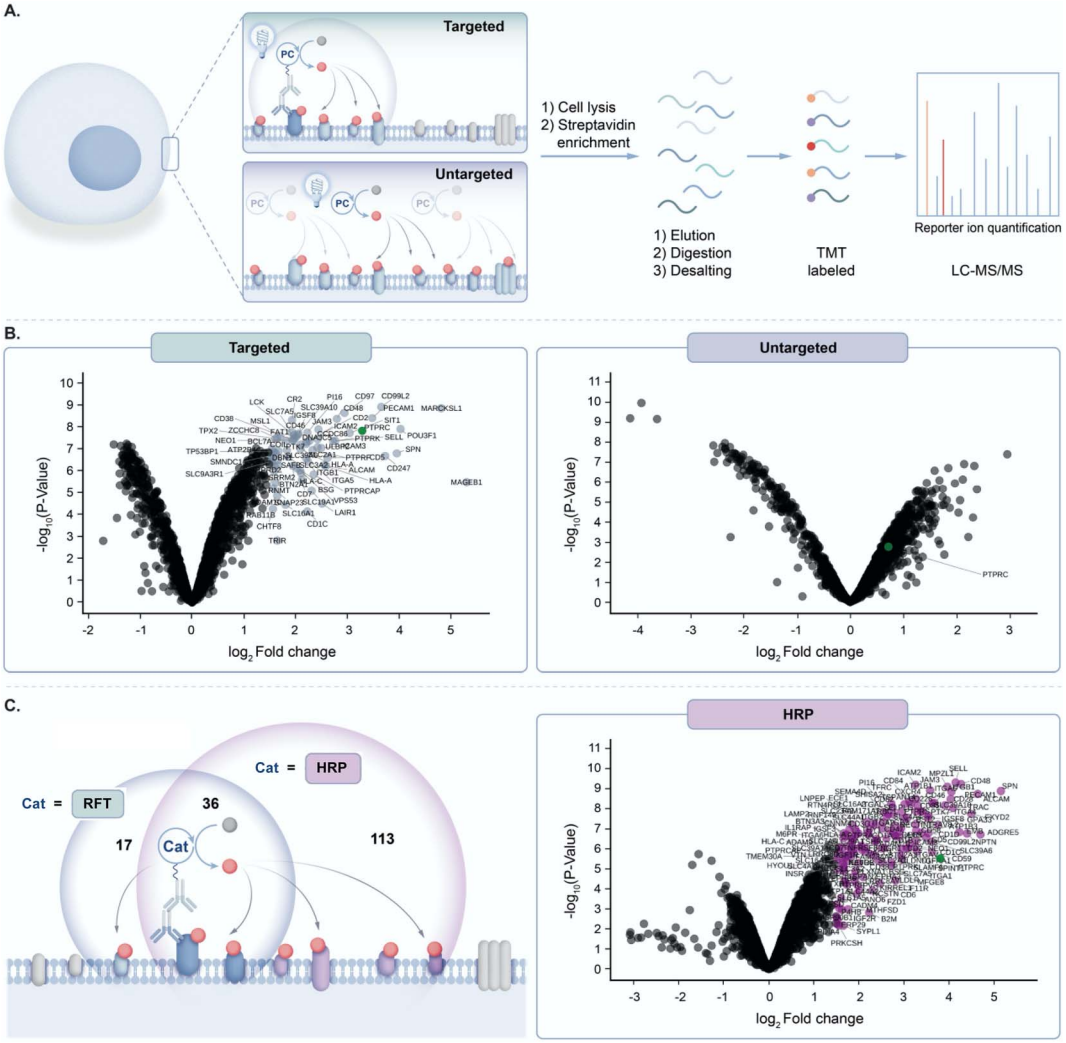

Fig. 2 (A) Schematic depicting targeted and untargeted labelling of CD45 (PTPRC) on the surface of Jurkat cells. Cells are labeled with an anti-CD45 primary antibody/secondary antibody **RFT** photocatalyst conjugate (targeted) or with free **RFT** photocatalyst (untargeted) followed by cell lysis, protein enrichment and digestion, and LC-MS/MS-based proteomic analysis. (B) Left, volcano plot of statistical significance *vs.* fold-enrichment for CD45-targeted *vs.* isotype-targeted biotinylation on Jurkat cells using an anti-CD45 primary antibody/secondary antibody **RFT** conjugate with 10 minutes of visible light activation in the presence of biotin tyramide. Significantly enriched proteins (p-value < 0.05 and $\log_2$ FC > 1.5) are indicated in light blue and CD45 (PTPRC) is labeled in green ($n = 3$ experiments). Right, volcano plot of statistical significance *vs.* fold-enrichment of free **RFT** photocatalyst and biotin tyramide *vs.* biotin tyramide only on Jurkat cells after 10 minutes of visible light activation. CD45 (PTPRC) is labeled in green ($n = 3$ experiments). (C) Left, schematic depicting CD45 targeted labelling between **RFT** and peroxidase (HRP)-based methods. Circles reflect a Venn diagram of the significantly enriched proteins from targeted labelling with HRP (purple circle, (C) right panel) or **RFT** (light blue circle, Fig. S2†). Right, volcano plot of statistical significance *vs.* fold-enrichment for CD45-targeted *vs.* isotype-targeted biotinylation on Jurkat cells using an anti-CD45 primary antibody/secondary antibody peroxidase conjugate (HRP) or isotype/secondary antibody peroxidase conjugate with 1 minute of labelling in the presence of biotin tyramide and hydrogen peroxide. Significantly enriched proteins (p-value < 0.05 and $\log_2$ FC > 1.5) are indicated in purple and CD45 (PTPRC) is labeled in green ($n = 3$ experiments).

excited state lifetimes and tunable redox potentials,[18–20] however, more bio-compatible photocatalysts such as **RFT** are desirable in protein labelling.[21] We explored **RFT** photochemistry and found several pathways by which phenoxyl radicals, from tags and tyrosine, could be generated. The multiple pathways that generate phenoxyl radicals support evidence of radical–radical recombination as a likely mechanism in these systems.

The photocatalytic cycle begins with blue light absorption by **RFT** followed by formation of a triplet excited state, ^{3}**[RFT]***. We observed ^{3}**[RFT]*** to display a relatively long excited state lifetime of 12 μs in deoxygenated solution, as determined by following its characteristic absorption at 700 nm in laser-flash photolysis experiments (Fig. 4A).

Due to their oxidizing nature, flavin-based triplet excited states can initiate radical chemistry.[22] In our system, phenol-containing tags or tyrosines in a protein will be rapidly oxidized by ^{3}**[RFT]*** to generate phenoxyl radicals. The rate constant (k_q) for this bimolecular process was determined by Stern–Volmer kinetics (Fig. 4B), which shows the oxidation of

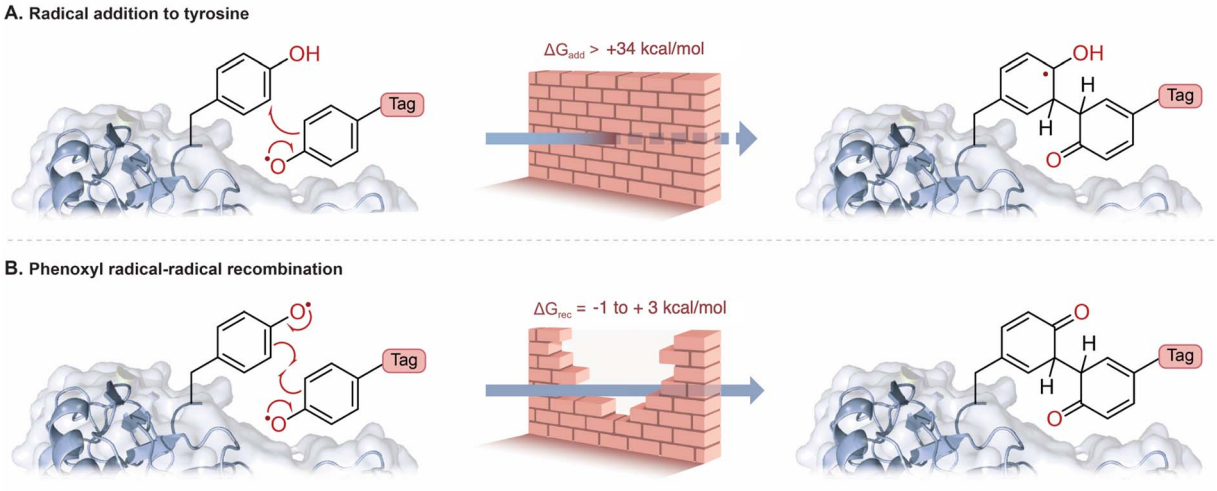

Fig. 3 (A) The addition of a phenoxyl radical tag to tyrosine is highly unfavorable (Table S10†). (B) Radical–radical recombination of phenoxyl radicals is more favorable, and rearromatization leads to a strong covalent bond (Table S9†). The relative rate constants were estimated according to Eyring's equation (see ESI† for details).

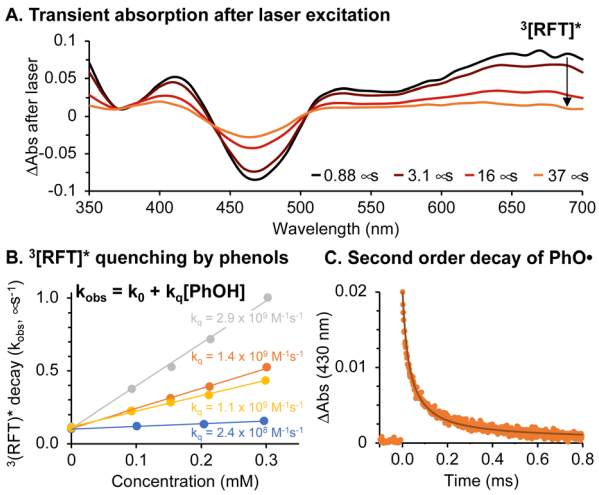

Fig. 4 (A) Transient absorption of RFT (0.06 mM) in deoxygenated acetonitrile : water (1 : 1) following 355 nm laser excitation. (B) Stern–Volmer quenching of ^{3}[RFT]* with 2,6-dimethoxyphenol (grey), biotin tyramide (orange), Ac–Tyr–NHMe (yellow) and BSA (blue). (C) Transient absorption of phenoxyl radicals from biotin tyramide and fit to second order decay kinetics (see ESI and Fig. S17† for details).

phenols with ^{3}[RFT]* to be fast in measured examples (10^8 to 10^9 M^{-1} s^{-1}) (Table S2†). When generated in laser flash photolysis experiments, phenoxyl radicals display a typical 2nd order decay as shown in Fig. 4C since they undergo a radical–radical recombination as their main decay pathway.

In the absence of oxygen, ^{3}[RFT]* will quickly be reduced by phenols, either from a tag or tyrosine group (Fig. 5A, Table S5†). The transient absorption of ^{3}[RFT]* at 700 nm rapidly decays in the presence of phenols to form a relatively stable intermediate with an absorption centered at 600 nm (Fig. 5B). We identify this peak as the semi reduced form, **H-RFT**$^\bullet$, with supporting evidence provided by TD-DFT predicted spectra (Fig. 5D). Semi-reduced flavins with similar chemical structures absorb in the same region.[22] Both transient absorption peaks associated with ^{3}[RFT]* and **H-RFT**$^\bullet$ are strongly attenuated by the introduction of oxygen (Fig. 5C).

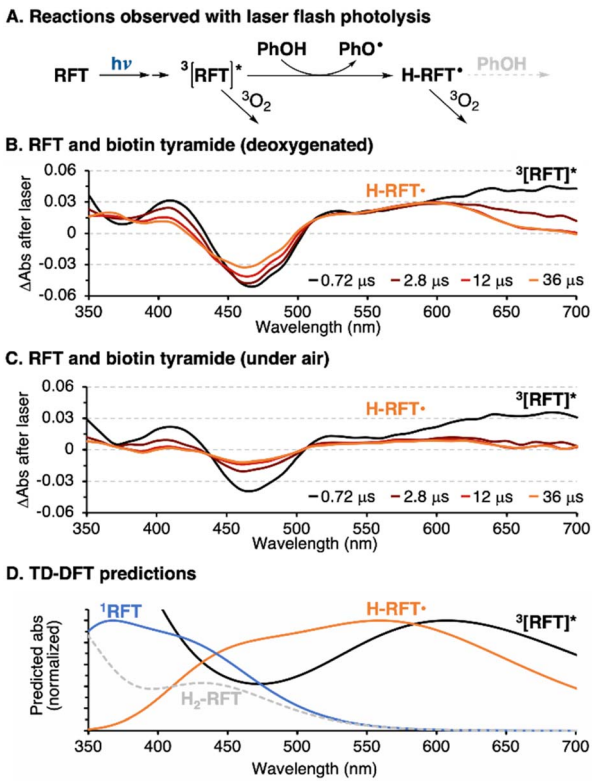

Fig. 5 (A) Reactions observed by laser-flash photolysis. (B) Transient absorption of RFT (0.06 mM) and biotin tyramide (0.3 mM) in the absence of oxygen after a 355 nm laser pulse. (C) Transient absorption of the same RFT (0.06 mM) and biotin tyramide (0.3 mM) solution open to air. (D) TD-DFT predicted absorption spectra of ground state RFT (blue), ^{3}[RFT]* (black), H-RFT$^\bullet$ (orange) and H_2-RFT (dashed grey).

We applied this photocatalytic coupling method on nucleophilic phenol substrates and tyrosine containing peptides where we observed tyrosine–phenol cross-coupling in moderate yields (Fig. S3 and Table S4†). During the optimization of our synthetic method, we found oxygen to be crucially important in maximizing the conversion efficiency (Table S4†). While the synthetic and protein labelling conditions differ in phenol type and concentration, this observation led us to investigative the role oxygen plays in the overall reaction mechanism.

Flavins are well-known singlet oxygen ($^1O_2$) sensitizers[22] and $^1O_2$ can oxidize phenols to phenoxyl radicals.[24–27] Using competitive kinetics with the probe 9,10-diphenylanthracene (**DPA**),[23] we measured the rate constant for the reaction of $^1O_2$ with electron rich phenols and a tyrosine analog to be $\sim 10^7$ M^{-1} s^{-1} (Fig. S24†). The H-abstraction from phenols by $^1O_2$ is calculated to be favorable with a ΔG_{DFT} from −12.3 to −18.0 kcal mol^{-1} (Table S7†).

Oxygen also plays a role in the photocatalytic turnover of **RFT**. Following excitation, ^{3}**[RFT]*** will react with phenols to form phenoxyl radicals and **H-RFT**$^\bullet$. Two pathways to regenerate **RFT** from **H-RFT**$^\bullet$ are considered. As often proposed in the literature for flavins, **H-RFT**$^\bullet$ can be further reduced to **H_2-RFT**,[11,22,28] however, we calculate this reduction to be significantly unfavorable in our system. Phenoxyl radical generation from the reaction between phenols and **H-RFT**$^\bullet$ gave ΔG_{DFT} values in the range of +19.4 to +25.2 kcal mol^{-1} (Table S6†). A second pathway to regenerate **RFT** from **H-RFT**$^\bullet$ bypasses the need to generate **H_2-RFT**. In the proposed mechanism (Fig. 6A), oxygen will directly oxidize **H-RFT**$^\bullet$ back to **RFT** with the formation of HOO$^\bullet$. This pathway has a more favorable ΔG_{DFT} of +4.99 kcal mol^{-1} than the full reduction (ΔG_{DFT} > +17 kcal mol^{-1}).

The detection of H_2O_2 as a by-product has been used as evidence for the catalytic cycle to involve **H_2-RFT**.[16] Indeed, the reduction of **H_2-RFT**, in a presumably multistep process, could favorably generate H_2O_2 in the presence of oxygen (ΔG_{DFT} = −23.4 kcal mol^{-1}). However, H_2O_2 can also be generated in pathways that do not include **H_2-RFT**. The reaction of $^1O_2$ with phenols will generate HOO$^\bullet$ as could the reaction of $^3O_2$ with **H-RFT**$^\bullet$. Both H-abstraction by HOO$^\bullet$ and recombination of two HOO$^\bullet$ can explain the presence of H_2O_2.

Finally, as proposed in Fig. 6B the phenoxyl radicals will recombine and favourably tautomerize (ΔG_{DFT} = −1 to +3 kcal mol^{-1} and ∼−36 kcal mol^{-1}, for each step respectively. See Table S9†).

Traditionally, the need for two radicals to recombine in a synthetically useful transformation is rare—the concentration of transient radicals is often too low to explain high yielding reactions. In this case, however, the persistence of phenoxyl radicals is well-documented—several antioxidants are based on phenoxyl radical's lack of side-reactions.[29] In biological systems, phenoxyl radicals are relatively persistent due to their low reactivity with oxygen and their inability to perform H-abstraction with most biomolecules—their estimated lifetime is ∼0.1 ms in cell media.[8]

The proposed mechanism described herein helps explain the success of phenoxyl radical labelling methods. Radical–radical recombination follows bimolecular kinetics, and the efficiency of this process will dramatically decrease as the distance increases away from the photochemical source of phenoxyl radicals. Another important factor in the success of this protein tagging method is the strength of the bonds formed. Radical–radical recombination becomes more predominant with increasing radical persistence; however, the recombination of persistent radicals can lead to weak and reversible bonds as is the case for certain carbon-centered radicals.[30] The recombination of phenoxyl radical is followed by tautomeric aromatization leading to bond strengthening. Altogether, these mechanistic insights will be an important consideration as different tag motifs are considered in photochemical protein tagging. Furthermore, the radical–radical

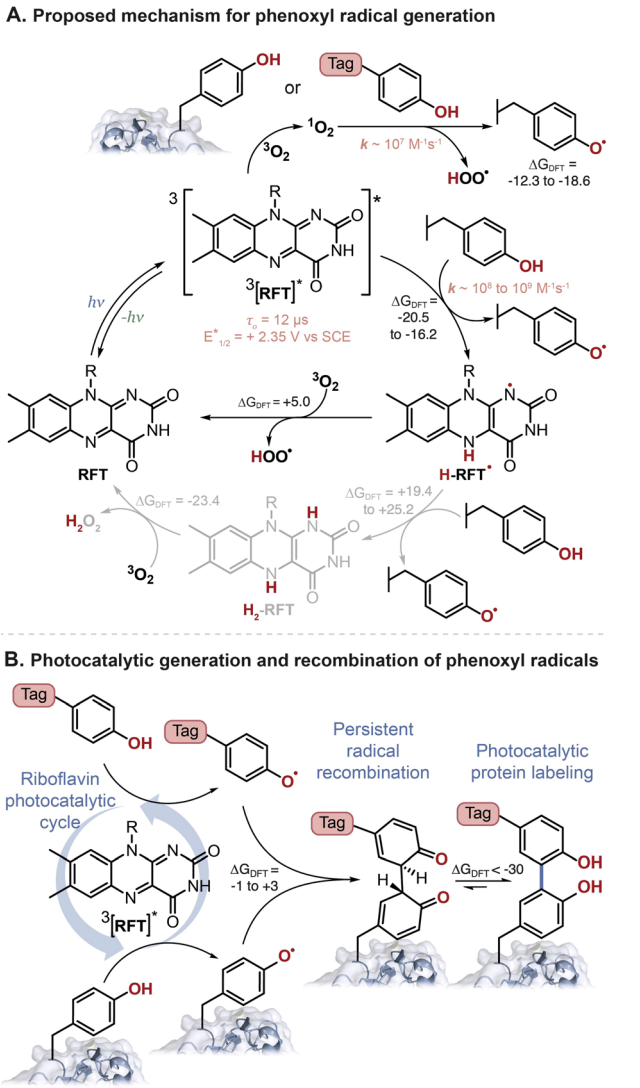

Fig. 6 (A) Proposed photocatalytic reaction mechanism for the generation of phenoxyl radicals from tyrosine-containing protein and phenol-containing tag molecules. (B) Phenoxyl radical are persistent radicals, and as such will recombine followed by rearomatization, as the preferred mechanism for phenol–phenol coupling. ΔG_{DFT}, shown in kcal mol^{-1}, were calculated using B3LYP-D3BJ/6-311+G(2d,2p)//CPCM(H_2O) with various phenols (see ESI† for details).

recombination mechanism described here might be a potential pathway that occurs in the case of peroxidase-based labelling systems.[31,32]

Conclusion

We envision that the insights gained from our mechanistic analysis will lead to improved catalytic performance of these flavin-based systems and further encourage the development of new and effective light-mediated labelling strategies in the field of chemical biology.

Data availability

Computational data is resumed in the ESI.† No other data in data repositories.

Author contributions

The manuscript was written by T. O. H., R. C. O., O. O. F. and M. F. All authors have given approval to the final version of the manuscript.

Conflicts of interest

T. R. R., K. A. R., R. C. O., and O. O. F. were employed by Merck Sharp & Dohme Corp., a subsidiary of Merck & Co., Inc., Rahway, NJ, USA during the experimental planning, execution and/or preparation of this manuscript.

Acknowledgements

We gratefully acknowledge NSERC for funding in the form of a Discovery Grant to M. F. (RGPIN-2016-06773). We are grateful to NanoQAM and to Compute Canada and Gaussian for computational resources.

Notes and references

1 K. A. Ryu, C. M. Kaszuba, N. B. Bissonnette, R. C. Oslund and O. O. Fadeyi, Interrogating biological systems using visible-light-powered catalysis, *Nat. Rev. Chem.*, 2021, **5**, 322–337.

2 M. Müller, F. Gräbnitz, N. Barandun, Y. Shen, F. Wendt, S. N. Steiner, Y. Severin, S. U. Vetterli, M. Mondal, J. R. Prudent and R. Hofmann, Light-mediated discovery of surfaceome nanoscale organization and intercellular receptor interaction networks, *Nat. Commun.*, 2021, **12**, 7036.

3 B. F. Buksh, S. D. Knutson, J. V. Oakley, N. B. Bissonnette, D. G. Oblinsky, M. P. Schwoerer, C. P. Seath, J. B. Geri, F. P. Rodriguez-Rivera, D. L. Parker and G. D. Scholes, μMap-Red: Proximity Labelling by Red Light Photocatalysis, *J. Am. Chem. Soc.*, 2022, **144**, 6154–6162.

4 R. C. Oslund, T. Reyes-Robles, C. H. White, J. H. Tomlinson, K. A. Crotty, E. P. Bowman, D. Chang, V. M. Peterson, L. Li, S. Frutos, M. Vila-Perello, D. Vlerick, K. Cromie, D. H. Perlman, S. Ingale, S. D. O'Hara, L. R. Roberts, G. Piizzi, E. C. Hett, D. J. Hazuda and O. O. Fadeyi, Detection of Cell-Cell Interactions *via* Photocatalytic Cell Tagging, *Nat. Chem. Biol.*, 2022, **18**, 850–858.

5 H. Wang, Y. Zhang, K. Zeng, J. Qiang, Y. Cao, Y. Li, Y. Fang, Y. Zhang and Y. Chen, Selective Mitochondrial Protein Labelling Enabled by Biocompatible Photocatalytic Reactions inside Live Cells, *JACS Au*, 2021, **1**, 1066–1075.

6 T. Tamura, M. Takato, K. Shiono and I. Hamachi, Development of a photoactivatable proximity labelling method for the identification of nuclear proteins, *Chem. Lett.*, 2020, **49**, 145–148.

7 A. D. Trowbridge, C. P. Seath, F. P. Rodriguez-Rivera, B. X. Li, B. E. Dul, A. G. Schwaid, B. F. Buksh, J. B. Geri, J. V. Oakley, O. O. Fadeyi, R. C. Oslund, K. A. Ryu, C. White, T. Reyes-Robles, P. Tawa, D. L. Parker Jr and D. W. C. MacMillan, Small molecule photocatalysis enables drug target identification *via* energy transfer, *Proc. Natl. Acad. Sci. U. S. A.*, 2022, **119**, e2208077119.

8 J. B. Geri, J. V. Oakley, T. Reyes-Robles, T. Wang, S. J. McCarver, C. H. White, F. P. Rodriguez-Rivera, D. L. Parker, E. C. Hett, O. O. Fadeyi, R. C. Oslund and D. W. C. MacMillan, Microenvironment mapping *via* Dexter energy transfer on immune cells, *Science*, 2020, **367**, 1091–1097.

9 N. Tay, K. A. Ryu, J. Weber, A. Olow, D. Reichman, R. Oslund, O. O. Fadeyi and T. Rovis, Targeted Activation in Localized Protein Environments *via* Deep Red Photoredox Catalysis, *ChemRxiv*, 2021, preprint, DOI: **10.26434/chemrxiv-2021-x9bjv**, accessed 2022-07-28.

10 S. Sato and H. Nakamura, Ligand-Directed Selective Protein Modification Based on Local Single-Electron-Transfer Catalysis, *Angew. Chem., Int. Ed.*, 2013, **52**, 8681–8684.

11 B. X. Li, D. K. Kim, S. Bloom, R. Y. C. Huang, J. X. Qiao, W. R. Ewing, D. G. Oblinsky, G. D. Scholes and D. W. C. MacMillan, Site-selective tyrosine bioconjugation *via* photoredox catalysis for native-to-bioorthogonal protein transformation, *Nat. Chem.*, 2021, **13**, 902–908.

12 N. Stephanopoulos and M. B. Francis, Choosing an effective protein bioconjugation strategy, *Nat. Chem. Biol.*, 2011, **7**, 876–884.

13 V. Hung, N. D. Udeshi, S. S. Lam, K. H. Loh, K. J. Cox, K. Pedram, S. A. Carr and A. Y. Ting, Spatially resolved proteomic mapping in living cells with the engineered peroxidase APEX2, *Nat. Protoc.*, 2016, **11**, 456–475.

14 M. Tsushima, S. Sato and H. Nakamura, Selective Purification and Chemical Labelling of a Target Protein on Ruthenium Photocatalyst Functionalized Affinity Beads, *Chem. Commun.*, 2017, **53**, 4838–4841.

15 D. A. Fancy and T. Kodadek, Chemistry for the Analysis of Protein-Protein Interactions: Rapid and Efficient Cross-Linking Triggered by Long Wavelength Light, *Proc. Natl. Acad. Sci. U. S. A.*, 1999, **96**, 6020–6024.

16 K. A. Niederer, P. H. Gilmartin and M. C. Kozlowski, Oxidative Photocatalytic Homo-and Cross-Coupling of Phenols: Nonenzymatic; Catalytic Method for Coupling Tyrosine, *ACS Catal.*, 2020, **10**, 14615–14623.

17 P. Danaher, S. Warren, L. Dennis, L. D'Amico, A. White, M. L. Disis, M. A. Geller, K. Odunsi, J. Beechem and

S. P. Fling, Gene expression markers of tumor infiltrating leukocytes, *J. Immunother. Cancer*, 2017, **5**, 1–15.

18 A. Juneau, T. O. Hope, J. Malenfant, M. Mesko, J. McNeill and M. Frenette, Methods to Predict Potential Reagents in Iridium-Based Photoredox Catalysis Calibrated with Stern–Volmer Quenching Rate Constants, *ACS Catal.*, 2022, **12**, 2348–2356.

19 A. C. Hernandez-Perez and S. K. Collins, Heteroleptic Cu-based sensitizers in photoredox catalysis, *Acc. Chem. Res.*, 2016, **49**, 1557–1565.

20 F. Glaser and O. S. Wenger, Recent progress in the development of transition-metal based photoredox catalysts, *Coord. Chem. Rev.*, 2020, **405**, 213129.

21 Y. B. Lee, S. Lim, Y. Lee, C. H. Park and H. J. Lee, Green Chemistry for Crosslinking Biopolymers: Recent Advances in Riboflavin-Mediated Photochemistry, *Materials*, 2023, **16**, 1218.

22 (*a*) B. Zhuang, U. Liebl and M. H. Vos, Flavoprotein Photochemistry: Fundamental Processes and Photocatalytic Perspectives, *J. Phys. Chem. B*, 2022, **126**, 3199–3207; (*b*) D. Grosheva and T. K. Hyster, Light-driven flavin-based biocatalysis, *Flavin-Based Catalysis: Principles and Applications*, ed. R. Cibulka and M. Fraaije, Wiley-VCH Verlag GmbH & Co. KGaA, 2021, pp. 291–313, DOI: 10.1002/9783527830138.ch12.

23 S. P. Pitre, C. D. McTiernan, W. Vine, R. DiPucchio, M. Grenier and J. C. Scaiano, Visible-light actinometry and intermittent illumination as convenient tools to study $Ru(bpy)_3Cl_2$ mediated photoredox transformations, *Sci. Rep.*, 2015, **5**, 1–10.

24 M. C. DeRosa and R. J. Crutchley, Photosensitized singlet oxygen and its applications, *Coord. Chem. Rev.*, 2002, **233**, 351–371.

25 M. J. Thomas and C. S. Foote, Chemistry of singlet oxygen—XXVI. Photooxygenation of phenolsy, *Photochem. Photobiol.*, 1978, **27**, 683–693.

26 F. E. Scully Jr and J. Hoigné, Rate constants for reactions of singlet oxygen with phenols and other compounds in water, *Chemosphere*, 1987, **16**, 681–694.

27 J. Al-Nu'airat, B. Z. Dlugogorski, X. Gao, N. Zeinali, J. Skut, P. R. Westmoreland, I. Oluwoye and M. Altarawneh, Reaction of phenol with singlet oxygen, *Phys. Chem. Chem. Phys.*, 2019, **21**, 171–183.

28 W. Chen, J. J. Chen, R. Lu, C. Qian, W. W. Li and H. Q. Yu, Redox reaction characteristics of riboflavin: a fluorescence spectroelectrochemical analysis and density functional theory calculation, *Bioelectrochemistry*, 2014, **98**, 103–108.

29 G. W. Burton and K. U. Ingold, Vitamin E: application of the principles of physical organic chemistry to the exploration of its structure and function, *Acc. Chem. Res.*, 1986, **19**, 194–201.

30 M. Frenette, C. Aliaga, E. Font-Sanchis and J. C. Scaiano, Bond dissociation energies for radical dimers derived from highly stabilized carbon-centered radicals, *Org. Lett.*, 2004, **6**, 2579, DOI: 10.1021/ol049111j.

31 T. Michon, M. Chenu, N. Kellershon, M. Desmadril and J. Guéguen, Horseradish peroxidase oxidation of tyrosine-containing peptides and their subsequent polymerization: a kinetic study, *Biochemistry*, 1997, **36**, 8504–8513.

32 J. V. Oakley, B. F. Buksh, D. F. Fernández, D. G. Oblinsky, C. P. Seath, J. B. Geri, G. D. Scholes and D. W. C. MacMillan, Radius measurement *via* super-resolution microscopy enables the development of a variable radii proximity labelling platform, *Proc. Natl. Acad. Sci. U. S. A.*, 2022, **19**, e2203027119.